Quantum Electronics **50** (11) 1007–1014 (2020)

https://doi.org/10.1070/QEL17372

Specific features of fluorescence transfer in multiply scattering randomly inhomogeneous layers under intense laser pumping

D.A. Zimnyakov, S.S. Volchkov, L.A. Kochkurov, A.F. Dorogov

Abstract. **Based on the analysis of experimental data on the effect of the pulsed laser pump intensity on the spectral properties and the size of the fluorescent response zone in randomly inhomogeneous fluorescent layers, we found that the amplification of spontaneous and stimulated emission significantly affects the statistical properties of the propagation lengths of the fluorescent field partial components in the layers. The experiments are performed with layers of SiO_2 and TiO_2 nanoparticles saturated with rhodamine 6G, pumped by 532-nm laser radiation in the intensity range corresponding to the transient regime from excitation of spontaneous fluorescence to random lasing in the layer. The experimental data are compared with the results of statistical modelling of fluorescence transfer. It is shown that, even at a pump intensity below the random lasing threshold, the spontaneous emission amplification in a layer leads to a significant increase in the contributions to the fluorescence response from partial components with propagation lengths much larger than the layer thickness. This can be interpreted as a manifestation of the quasi-waveguide effect, in which the probability of propagation of diffuse fluorescence components along the layer over distances many times greater than its thickness and the size of the pumped region increases significantly with a decrease in the characteristic radiation amplification length in the layer.**

Keywords: *randomly inhomogeneous medium, fluorescence, laser pumping, random lasing, spontaneous emission, propagation length.*

1. Introduction

Various aspects of the light wave propagation in multiply scattering media have been studied over a hundred and fifty years. A sharp increase in interest in these studies falls on the period from the beginning of the eighties of the last century to the beginning of the 2000s and is due to several reasons. One of them was the creation and development of a number of effective methods for optical diagnostics of randomly inhomogeneous media (diffusing-wave spectroscopy, etc. [1–5]) for materials science and biomedical applications. The studies were also motivated by the idea of the possibility of obtaining localised states of light fields in strongly scattering randomly inhomogeneous media [6–8]. The hypothetical possibility of obtaining localised states of the electromagnetic field in randomly inhomogeneous media follows from the analogy between the solution of the wave equation for the electromagnetic field in such systems and the wave function of conduction electrons in amorphous conductors.

An interesting particular case of the propagation of light in randomly inhomogeneous media is the transfer of fluorescence excited by pumping a fluorophore contained in the medium by an external source. Fluorescent methods are widely used in modern biomedical diagnostics. Similar studies are related to the implementation and use of random lasing in randomly inhomogeneous media, predicted by V.S. Letokhov [9]. The peak of research activity in this area fell on the first decade of this century, and at present, the interest in them does not diminish, despite the lack of tangible results in the field of application of the effect. This interest is due to both possible diagnostic applications of the effect and the prospects for studying the features of nonlinear and resonant interactions of radiation with disordered ensembles of particles.

To date, the theory of cavityless lasing in randomly inhomogeneous media has been sufficiently developed and verified by experimental data (see, e.g., [10, 11]). In some papers, the effect of random lasing is considered in the context of achieving localised states of the light field in a pumped randomly inhomogeneous medium [11]. Despite the obvious successes in theoretical and experimental studies of this phenomenon, insufficient attention has been paid to its particular aspects. One of these aspects is related to the peculiarities of the statistics of the propagation lengths of the fluorescent field partial components through the medium in the transient regime between the spontaneous fluorescence response and the random lasing. Amplification of spontaneous emission even in the subthreshold regime within the framework of the concept of pumped medium negative absorption should cause an increase in the weight of the light field partial components, propagating through the medium over distances significantly exceeding its dimensions. The latter should lead to an increase in the contributions to the fluorescence response of photon ensembles with long times of residence in the medium. This,

D.A. Zimnyakov Yuri Gagarin State Technical University of Saratov, ul. Politekhnicheskaya 77, 410054 Saratov, Russia; Institute for Problems of Precision Mechanics and Control, Russian Academy of Sciences, ul. Rabochaya 24, 410028 Saratov, Russia; e-mail: zimnykov@mail.ru;
S.S. Volchkov, L.A. Kochkurov, A.F. Dorogov Yuri Gagarin State Technical University of Saratov, ul. Politekhnicheskaya 77, 410054 Saratov, Russia

Received 22 May 2020
Kvantovaya Elektronika **50** (11) 1007–1014 (2020)
Translated by V.L. Derbov

in particular, is evidenced by the results of reference-free low-coherence interferometry of fluorescent randomly inhomogeneous media [12, 13]. It was found that near the spectral maximum of the medium fluorescence response in the subthreshold regime, there is an increase in the ratio of the average propagation length of the fluorescent field partial components to its coherence length measured by narrow-band detection.

The aim of this work is to explore the specific features of fluorescence transfer in randomly inhomogeneous media due to negative absorption for pump regimes corresponding to the transition from spontaneous fluorescence to random lasing.

2. Experimental technique and results

A schematic of the setup for studying the fluorescence response of randomly inhomogeneous layers under laser pumping is shown in Fig. 1. The samples under study were layers of closely packed SiO_2 and TiO_2 particles saturated with an aqueous solution of rhodamine 6G. Pumping was carried out by pulsed radiation with $\lambda = 532$ nm and pulse duration $\tau_i = 10$ ns. The radiation source was a Lotis TII-2145-OPO laser; the pulse energy E_i on the sample surface was measured using a Gentec Maestro meter and varied from 0.04 to 20 mJ. The laser beam passed through a collecting lens with a focal length of 150 mm and hit the sample located at a distance of 70 mm from the beam waist. The pump zone diameter d_p was ~1.14 mm.

We investigated the size of the fluorescence response zones on the sample surface as a function of the pump intensity $I_p \approx 4E_i/(\pi d_p^2 \tau_i)$; the images of the zones were recorded using an Optronis-CamRecord CR3000-2 CMOS camera with macroscopic optics based on a Tamron objective. To cut off the pump radiation, an OS-13 filter was placed in front of the objective. Figures 2a and 2b show examples of images of the recorded response zones. The images were recorded under a single action of laser pulses on the samples, the frame recording being timed with the laser pulse (with the required delay). The estimation of the size of the zones was carried out as follows: The threshold value of the intensity of the fluorescent response corresponding to the border of the zone was taken equal to three times the value of the intensity recorded far from the zone of the response. Then the area was contoured with the subsequent counting of the number of pixels inside the contour. The radius of the response zone for a given pump intensity was determined as $r_f \approx \sqrt{N_p S_p/\pi}$, where N_p is the number of pixels within the contoured region, and S_p is the area covered by one pixel. Figure 2c shows the dependences of r_f on I_p for the samples under study. In the experiments, the fluorescence spectra of the samples were also recorded as a function of I_p using an Ocean Optics QE65000 spectrometer with a P200-2-UV-VIS fibre optic patchcord. The input end of the patchcord was located at a distance $z_f = 45$ mm from the surface satisfying the condition $z_f \approx r_c/\mathrm{NA}$, optimal for detecting fluorescence (r_c is the radius of the container with the sample, NA ≈ 0.22 is the numerical aperture of the patchcord). The fluorescence spectra were recorded under repetitively pulsed irradiation of the samples with a repetition rate of 10 Hz. Figure 3 shows the fluorescence spectra $I_f(\lambda)$ of the samples (Figs 3a, 3b) and rhodamine 6G solution (Fig. 3c). The dye solution in a closed 1-mm-thick cuvette was located in the area of the studied samples.

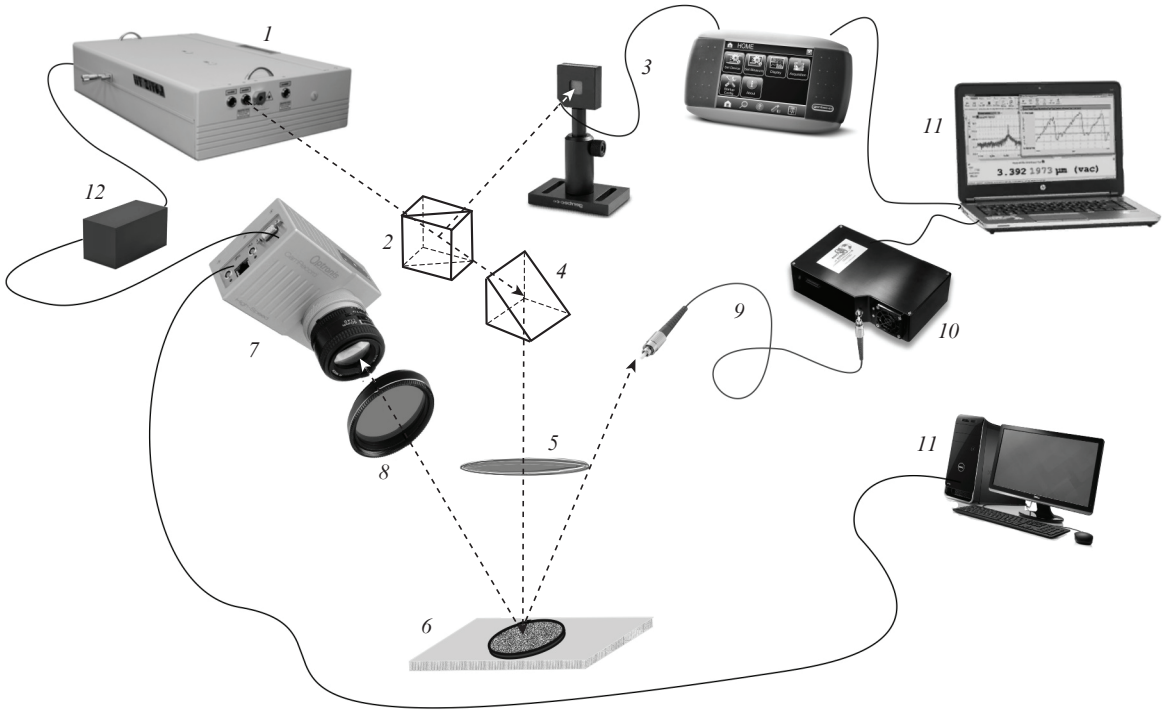

Figure 1. Experimental setup:
(*1*) laser; (*2*) beam splitter; (*3*) laser energy meter; (*4*) rotating prism; (*5*) collecting lens; (*6*) container with a sample; (*7*) CMOS camera; (*8*) filter blocking pump radiation; (*9*) fibre-optic patchcord; (*10*) spectrometer; (*11*) PC; (*12*) clock unit of CMOS camera and laser.

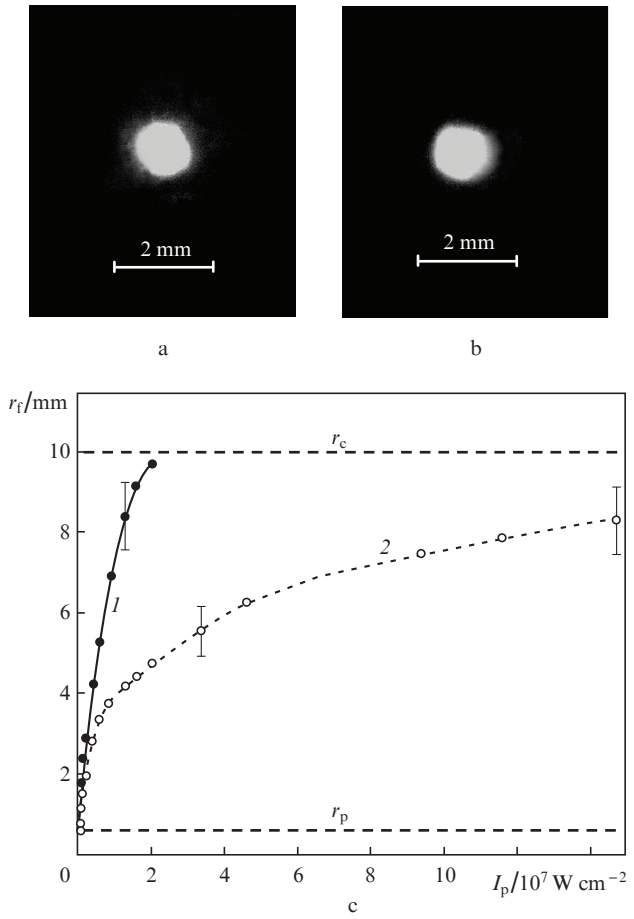

Figure 2. (a, b) Images of the fluorescence response zones at a pump intensity $I_p = 4.9 \times 10^5$ W cm^{-2} for (a) SiO_2 and (b) TiO_2 layers, as well as (c) the dependence of the fluorescence response zone radius on the pump intensity for (*1*) SiO_2 and (*2*) TiO_2 layers. Confidence intervals in Fig. 2c correspond to a significance level of 0.9 and characterise the scatter of values from sample to sample for a series of five measurements, and the horizontal dashed lines correspond to the radius of the pumping region r_p and the radius of the container r_c.

A characteristic feature is the transition to the random lasing regime for samples based on TiO_2 nanoparticles, which manifests itself in a decrease in the half-width of the fluorescence spectrum $\Delta\lambda_{0.5}$ with increasing I_p (Fig. 4). The lasing threshold, determined for TiO_2 samples from the position of the inflection point of the dependence $\Delta\lambda_{0.5} = f(I_p)$, was $\sim 8.2 \times 10^6$ W cm^{-2} [Fig. 4, curve (*1*)]. For samples based on SiO_2 nanoparticles, the transition to the lasing regime is absent up to $I_p \approx 2.2 \times 10^8$ W cm^{-2}, and the narrowing of the spectrum is insignificant in comparison with that for TiO_2 samples.

It is of fundamental importance to determine the thickness L and optical parameters (the transport length l^* of radiation propagation, the scattering anisotropy parameter g, and the effective refractive index n_{eff} (see, e.g., [14])) of the samples under study for the pump wavelength and in the wavelength range of the fluorescent response. The samples were prepared in metal containers in the form of washers 1 mm in height with an internal diameter 20 mm, fixed on 1-mm-thick glass substrates. The containers were filled with powders of TiO_2 [product No. 637254 from Sigma Aldrich, polydisperse TiO_2 nanoparticles (in the anatase

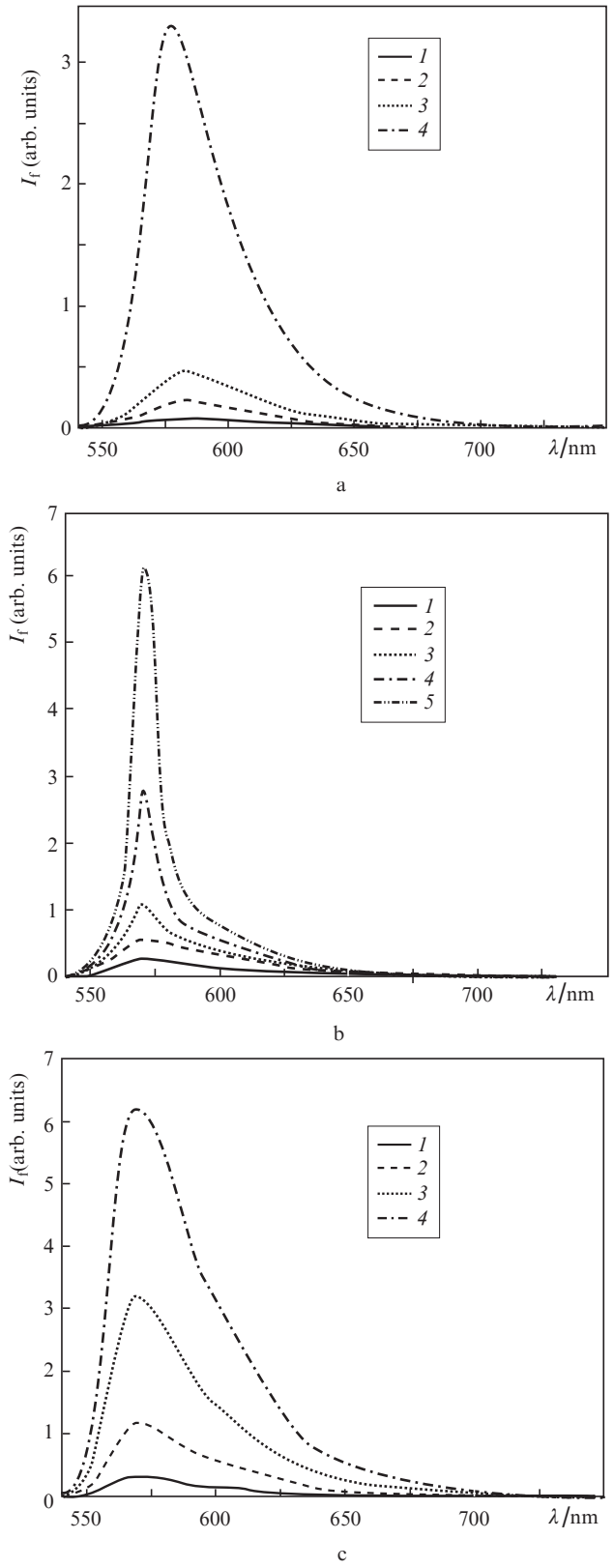

Figure 3. Fluorescence spectra of the studied samples under excitation at $\lambda = 532$ nm for (a) a SiO_2 layer with a rhodamine 6G solution at I_p = (*1*) 5.88×10^6, (*2*) 1.37×10^7, (*3*) 2.65×10^7, and (*4*) 1.96×10^8 W cm^{-2}, (b) a TiO_2 layer with a rhodamine 6G solution at I_p = (*1*) 2.94×10^6, (*2*) 5.88×10^6, (*3*) 1.37×10^7, (*4*) 2.65×10^7, and (*5*) 3.92×10^7 W cm^{-2}, as well as (c) a rhodamine 6G solution at I_p = (*1*) 1.18×10^6, (*2*) 2.45×10^6, (*3*) 4.41×10^6, and (*4*) 1.08×10^7 W cm^{-2}.

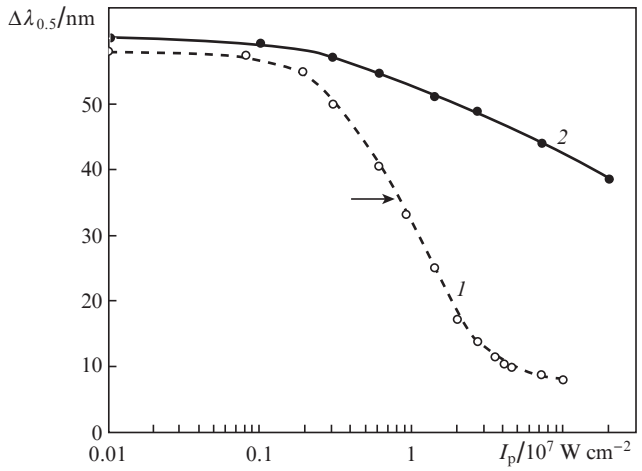

Figure 4. Dependences of the fluorescence spectra half-width on the pump radiation intensity for (*1*) TiO_2 and (*2*) SiO_2 layers. The arrow indicates the lasing threshold for TiO_2 layers.

modification) with an average size of $\bar{d}_{TiO_2} \leqslant 25$ nm and a bulk density of ~0.05 g cm^{-3}] and SiO_2 (product No. 637238 from Sigma Aldrich, polydisperse SiO_2 nanoparticles with a size $\bar{d}_{SiO_2} \approx 20$ nm and a bulk density of ~0.011 g cm^{-3}). The layers of particles were compacted and saturated with an aqueous solution of rhodamine 6G (the solution volume for one container was 100 μL). The thickness of the layers after shrinkage upon saturation with a solution was measured using an OSC1300SS optical coherence tomograph (Thorlabs, USA). The average value of L was 770 ± 24 μm for TiO_2 samples and 820 ± 26 μm for SiO_2 samples. The scatter of L values over the layer surface did not exceed ± 4%. Volumetric measurements showed that the volume fraction f of particles in the layers is ~0.2 for TiO_2 samples and ~0.1 for SiO_2 samples. A similar technique was used to prepare test samples of TiO_2 and SiO_2 saturated with distilled water, for which, using a Thorlabs IS236A integrating sphere, an Ocean Optics QE65000 spectrometer, and a broadband radiation source based on a halogen lamp, the diffuse transmission spectra were obtained in the wavelength range from 500 to 800 nm.

From the values of f and $\bar{d}$, the values of g and n_{eff} were estimated using the effective medium model in the coherent potential approximation [15, 16]. It was found that both systems under study are characterised by small values of the anisotropy parameter ($g < 0.2$), i.e., the radiation scattering character is close to isotropic. The effective refractive indices for liquid-saturated TiO_2 and SiO_2 samples were ~1.55 and ~1.38, respectively. From the obtained diffuse transmission spectra using the inverse Monte Carlo (MC) method for the samples under study, the values of l^* were estimated for the pump radiation wavelength and the wavelength corresponding to the maximum of the fluorescence response ($\lambda \approx$ 570 nm): $l^*_{532} \approx 500$ μm, $l^*_{570} \approx 550$ μm for the SiO_2 sample and $l^*_{532} \approx 2.5$ μm and $l^*_{570} \approx 4.0$ μm for the TiO_2 sample. Such significant differences are due to the large values of the scattering efficiency factor for TiO_2 nanoparticles as compared to SiO_2 nanoparticles. For the used solution of rhodamine 6G with a molar concentration of ~1.0×10^{-4} mol L^{-1}, the absorption coefficient at the pump wavelength was measured (~1.74 mm^{-1}).

3. Simulation of fluorescence transfer

The features of the fluorescence propagation in the pumped layers were analysed theoretically using the results of MC simulation of the interaction of pump radiation with the layers under study. We consider the following MC model: a pump photon enters a layer saturated with a fluorophore and, after passing a certain random distance in it, is absorbed by a fluorophore molecule. The excited molecule emits a fluorescence quantum that undergoes random walks until it leaves the layer through the upper (from the side of the pump source) or lower boundary. In the course of simulation, the number of fluorescence quanta $\Delta N_f/\Delta S_{ub}$ leaving the layer through a unit area at the upper boundary is determined, depending on the distance from the centre of the pump region, when $N_{ph} = 10^7$ pump photons fall into this region. We also determined the probability density sample distribution function $\rho(s)$ of fluorescent quanta that left the layer over the propagation lengths s in the layer. The distribution of the points of entry of pump photons into the layer over the surface of the pumped region is assumed to be uniform, and the total number of induced quanta of the fluorescent field is assumed to be proportional to the number of pump photons ($N_f \propto N_{ph}$). This assumption corresponds to the obtained experimental data on the linear fluorescence response of the samples under study in a sufficiently wide range of pump radiation intensities. The effect of an increase in the size of the fluorescence response zone r_f on the layer surface with an increase in the intensity I_p is illustrated in Fig. 5.

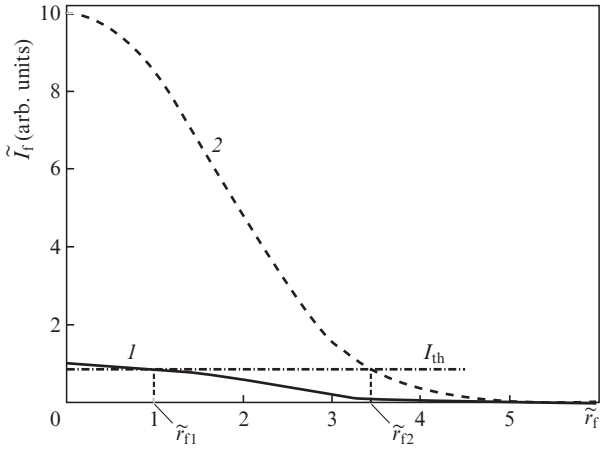

Figure 5. Illustration of the technique for reconstructing the normalised model dependence of the radius of the fluorescence response zone on the pump radiation intensity $\tilde{r}_f = f(\tilde{I}_p)$: the radial distributions of the fluorescence response intensity over the zone for the pump radiation intensity $I_{p1} = I_0$, at which the radius of the response zone is equal to the radius of the pump region (*1*), and intensity $I_{p2} = 10I_0$ (*2*); I_{th} is the intensity threshold for determining the radius of the response zone.

When simulating the transfer of fluorescent photons, the absorption index of the layers was taken to be zero, and the photon scattering was assumed to be isotropic, based on small values of the parameter g for the samples under study. The obtained model data on the effect of I_p on r_f for nonabsorbing layers were compared with the experimental results presented in Fig. 2 in order to analyse the possible manifestation of negative absorption of the layers in the fluorescence response as a function of I_p and l^*. The assumption about

zero absorption of the samples, $\mu_a = 0$ (without taking the possible negative absorption into account), is justified, since near the maximum of the spectral response of fluorescence the absorption indices of both SiO_2 and TiO_2 matrices (μ_{am}) and fluorophore (μ_{ad}) satisfy the condition $l^* \ll \mu_{am}^{-1}, \mu_{ad}^{-1}$. In the presence of negative absorption of fluorescence in the layers due to the amplification of spontaneous or stimulated emission, the probability density function $\rho(s)$, obtained at zero absorption, must be renormalised taking into account the Bouguer factor:

$$\tilde{\rho}(s) = \rho(s)\exp(\mu_a s) \Big/ \int_0^\infty \rho(s)\exp(\mu_a s)\,\mathrm{d}s. \qquad (1)$$

During the simulation, possible reflections of fluorescent photons from the boundaries into the depths of the layers due to the difference in the refractive indices of the layer and the free space above it were taken into account. When simulating the distributions of elementary sources of fluorescent photons induced by pump radiation, we used model parameters found from experimental data (see above).

Figure 6 shows the intermediate results of MC simulation: the radial distributions of elementary sources of fluorescent quanta in dimensionless coordinates z/L, r/L for SiO_2 and TiO_2 samples (z is the distance from the layer surface, and r is the distance from the pump beam axis) and normalised impulse response functions $\Psi(r/L) = [\Delta N_f(r/L)/\Delta S_{ub}]/[\Delta N_f(0)/\Delta S_{ub}]$ for surface distributions of fluorescence intensity upon excitation by a packet of pump photons, entered at the point with coordinates $z = 0$ and $r = 0$. Model radial distributions of the fluorescence response intensity, used to reconstruct the dependences $\tilde{r}_f = f(\tilde{I}_p)$ (Fig. 5), can be obtained by numerical integration of the functions $\Psi(r/L)$ over the volume of the pumped region or directly during the MC modelling, as in our case. In SiO_2 layers, the spatial distributions of fluorescence sources are much more delocalised than in TiO_2 layers, due to a much larger value of l^* (Fig. 6a). In the first case, the average pump energy density in the region of exposure to laser radiation is less than the corresponding value for TiO_2 layers by more than an order of magnitude. The delocalisation of the fluorescence source in the SiO_2 layers leads to an additional broadening of the impulse response function $\Psi(r/L)$ (Fig. 6b) and to a significantly greater 'smearing' of the spatial distributions of the fluorescence intensity $I_f(r)$ (Figs 2a and 2b).

In Fig. 7, the normalised model dependences $\tilde{r}_f = f(\tilde{I}_p)$ for $\mu_a = 0$ are compared with the normalised experimental values of the radius of the response zone depending on I_p (Fig. 2c). The normalisation was carried out as follows: $\tilde{r}_f = r_f/r_p$, $\tilde{I}_p = I_p/I_p(r_f = r_p)$, where $I_p(r_f = r_p)$ is the value of the pump radiation intensity at which the radius of the fluorescent zone r_f is equal to the radius of the pumped region r_p.

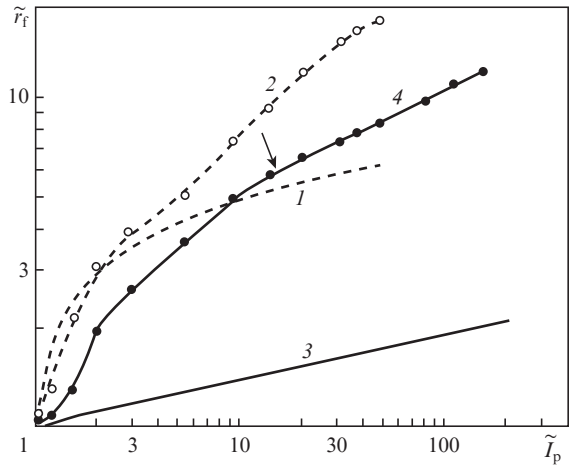

Figure 7. (*1*, *3*) Model and (*2*, *4*) experimental dependences of the normalised radius of the fluorescence response zone on the normalised pump intensity for (*1*, *2*) SiO_2 and (*3*, *4*) TiO_2 layers. For dependence *4*, the arrow indicates the threshold of random lasing in the TiO_2 layers under study.

4. Discussion of results

Comparison of model and experimental data on the effect of I_p on r_f allows one to make a conclusion that the negative

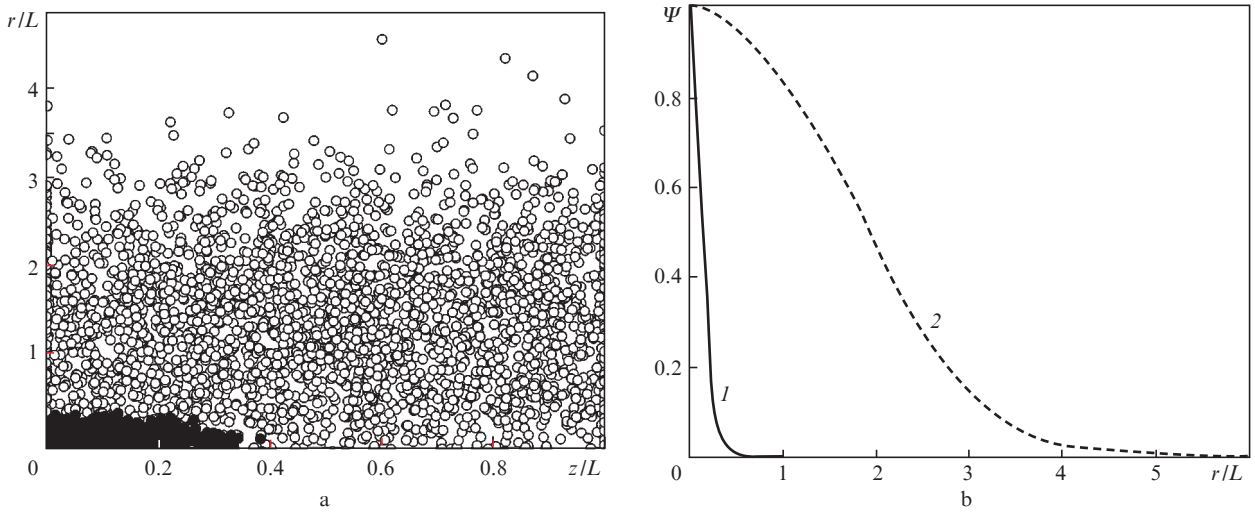

Figure 6. (a) Model radial distributions of elementary fluorescence sources in (○) SiO_2 and (●) TiO_2 layers and (b) normalised model impulse response functions $\Psi(r/L)$ for surface distributions of fluorescence intensity in (*1*) TiO_2 and (*2*) SiO_2 layers.

absorption (amplification) of fluorescence in the layers under study plays an essential role even at pump intensities below the threshold for random lasing. This fact manifests itself in higher, compared to model systems, rates of increase in $\tilde{r}_f$ with increasing $\tilde{I}_p$ for the samples under study, especially for TiO_2 layers. The enhancement of spontaneous and stimulated (near and above the lasing threshold) fluorescence should lead to an increase in the contribution of the partial components of the light field with lengths s that significantly exceed the thickness of the layers. These components diffusely propagate in the layers at distances that are many times greater than the size of the pumped region.

From the obtained fluorescence spectra $I_f(\lambda)$ for the samples under study and a solution of rhodamine 6G (Fig. 3), the effective cross section of fluorescence emission can be determined [17, 18]:

$$\sigma_e(\lambda) = \frac{1}{\tau_{lt}} \frac{I_f(\lambda)\lambda^5}{8\pi c n^2 \int I_f(\lambda)\lambda d\lambda}, \quad (2)$$

where τ_{lt} is the lifetime of the excited fluorescent state; n is the refractive index of the medium; and c is the speed of light. In accordance with [19], for rhodamine 6G, in the absence of nonlinear and concentration effects, the value of τ_{lt} can be taken equal to $\sim 4 \times 10^{-9}$ s, and the refractive index of an aqueous solution of the dye at moderate concentrations $\sim$1.34 [20]. Figure 8 shows the spectra of the effective emission cross section $\sigma_e(\lambda)$ for aqueous solutions of rhodamine 6G in a wide range of pump energies calculated using Eqn (2) for two values of the dye concentration, the initial concentration used in the preparation of samples, and 65% from the initial one. Note the almost identical shapes and maxima of the curves obtained, despite significant differences in the pump energies and dye concentrations.

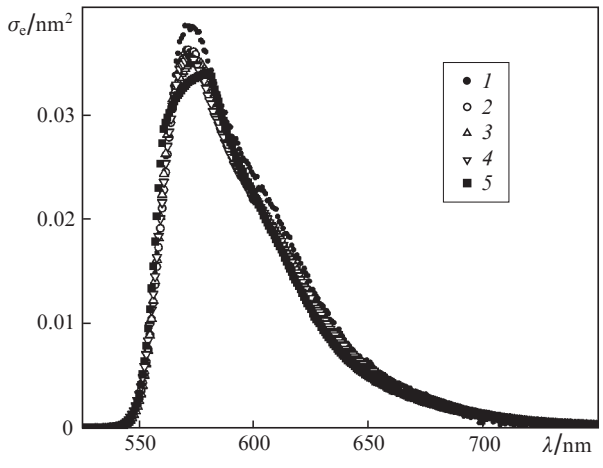

Figure 8. Spectra of the effective cross section of fluorescence emission of rhodamine 6G solutions with different concentrations at different pump radiation intensities: (*1*) 100%, 7.84×10^5 W cm^{-2}; (*2*) 100%, 2.45×10^6 W cm^{-2}; (*3*) 100%, 1.08×10^7 W cm^{-2}; (*4*) 65%, 2.45×10^6 W cm^{-2}; and (*5*) 65%, 3.14×10^7 W cm^{-2}.

The negative absorption index can be assumed proportional to $\sigma_e(\lambda)$ and the concentration n_d of the dye molecules, $\mu_a(\lambda) = -\sigma_e(\lambda)n_d$. When radiation propagates in a randomly inhomogeneous medium, the amplification of spontaneous radiation leads to a significant increase in the contributions of the partial components of the fluorescent field with propagation lengths $s > \mu_a^{-1}(\lambda)$ to the recorded signal. This effect manifests itself, in particular, in the earlier considered [12, 13] suppression of the stochastic interference component of the fluorescence response for wavelengths near the wavelength at which its maximum value is reached, with reference-free low-coherence interferometry of fluorescent randomly inhomogeneous layers. For example, at $\sigma_{e\,max} \approx 0.04$ nm^2 (Fig. 8) and $n_d \approx 1.5 \times 10^{-4}$ nm^{-3} (which corresponds to a dye concentration of 2.5×10^{-4} mol L^{-1} [13]), the characteristic emission enhancement length $(\sigma_{e\,max} n_d)^{-1} \approx 170$ μm even at low intensities of continuous pump radiation (a few W cm^{-2}). This is comparable to the characteristic propagation lengths of the light field partial components in scattering layers with thicknesses of the order of several hundred microns.

The presence of a fluorophore in structurally disordered matrices of closely packed nanoparticles leads to changes in the spectra of the effective emission cross section compared to those for pumping outside the matrix, as well as in the $\sigma_e(\lambda)$ dependence at different pump intensities (Fig. 8). Since the lifetime τ_{lt} in such spatially confined systems essentially depends on the pump radiation intensity and the structural properties of the matrix, and in our experiments measurements of the fluorescence decay kinetics were not carried out, only the values of the spectral factor

$$\Omega(\lambda) = I_f(\lambda)\lambda^5 \Big/ \int I_f(\lambda)\lambda d\lambda,$$

that enters Eqn (2) were considered when analysing the data. The dependences $\Omega(\lambda)$ for the SiO_2 and TiO_2 layers at different I_p are shown in Fig. 9. Note the slightly lower values of $\Omega(\lambda)$ for TiO_2 layers at $I_p < 6 \times 10^6$ W cm^{-2} compared to SiO_2 layers and rhodamine 6G solutions outside the matrices (Fig. 8). In this case, the lifetime of excited fluorescent states in spatially confined systems with small values of the characteristic scattering volume ($\sim l^{*3}$) is much shorter than the analogous parameter in the fluorophore outside the matrix [21].

It is of interest to compare the results obtained by exciting random lasing in TiO_2 layers with the condition for reaching the critical size of the pumped randomly inhomogeneous medium [9, 22]. When pumping an amplifying randomly inhomogeneous layer, its critical thickness is determined as $L_{cr} = \pi\sqrt{l^* l_g/3}$, where l_g is the propagation length of the partial component corresponding to an increase in its intensity by a factor of e. Let $l_g \approx [\sigma_e(\lambda)n_d]^{-1}$, then, in accordance with Fig. 9b, at the maximum fluorescence efficiency in TiO_2 layers near the lasing threshold $\Omega_{max} \approx 1.4 \times 10^9$ nm^3. Assuming, as before, the lifetime of the excited states of dye molecules below and close to the lasing threshold equal to $\sim 4 \times 10^{-9}$ s, we obtain $l_g \approx 830$ μm for the concentration of dye molecules used ($n_d \approx 6.0 \times 10^{-5}$ nm^{-3}). The specified value can be compared with $l_g = 3L_{cr}^2/(\pi^2 l^*)$. It should be borne in mind that, in TiO_2 layers, fluorescence is excited not over the entire layer thickness, but in a thin near-surface layer with a thickness essentially less than d_p.

The inset in Fig. 10 shows the normalised distribution of the density of elementary fluorescence sources over the depth of the pumped TiO_2 layer, found by MC simulation. Assuming that the effective thickness of the active region is $\Delta z_f \approx L_{cr} \approx 0.148L \approx 114$ μm and $l^*_{570} \approx 4$ μm, we obtain $l_g \approx 990$ mm, which, taking into account the assumptions made, is quite

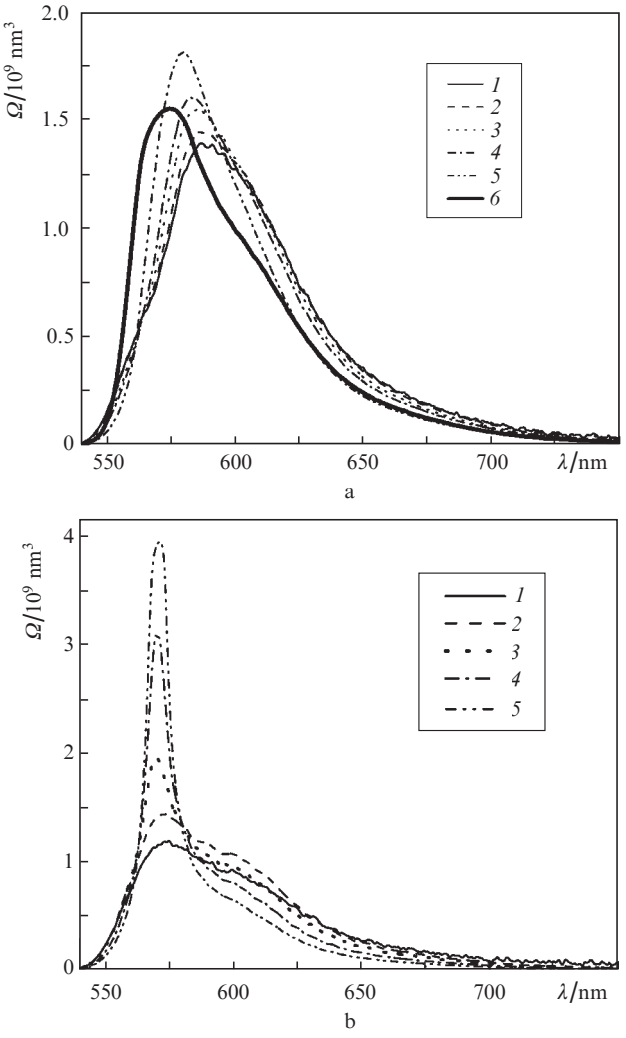

Figure 9. Spectral distributions $\Omega(\lambda)$ (a) for the SiO_2 layer at I_p = (*1*) 2.94×10^6, (*2*) 2.94×10^6, (*3*) 1.37×10^7, (*4*) 2.65×10^7 and (*5*) 1.96×10^8 W cm^{-2} and for the used rhodamine 6G solution at I_p = 1.08×10^7 W cm^{-2} [(*6*), for comparison], as well as (b) for the TiO_2 layer at I_p = (*1*) 9.8×10^5, (*2*) 5.88×10^6, (*3*) 1.37×10^7, (*4*) 2.65×10^7 and (*5*) 3.92×10^7 W cm^{-2}.

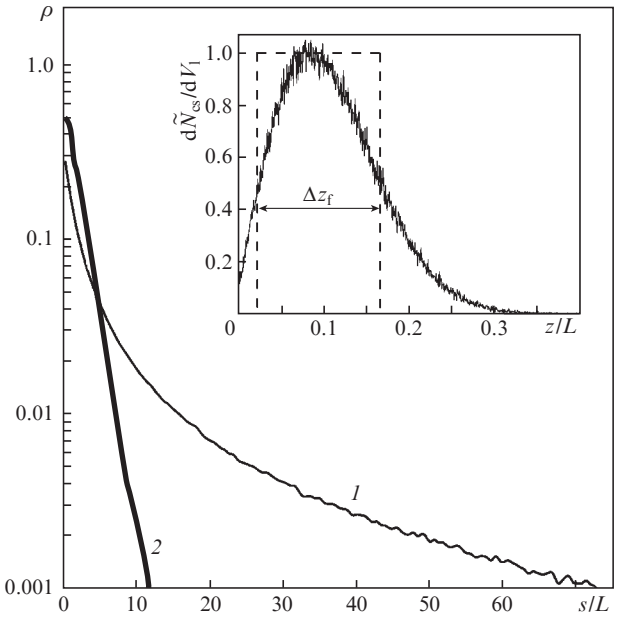

Figure 10. Model probability density functions of the propagation lengths of the partial components in (*1*) SiO_2 and (*2*) TiO_2 layers at zero absorption. The inset shows the normalised model distribution of the density of elementary fluorescence sources $d\tilde{N}_{es}/dV_1$ over the depth of the TiO_2 layer (dV_1 is the elementary volume in the layer); effective core thickness $\Delta z_f = \int_0^1 (d\tilde{N}_{es}/dV_1)d(z/L)$.

close to the above estimate made using the values Ω_{max} and n_d. For SiO_2 layers, in accordance with approximate estimates, the critical thickness at low pump radiation intensities is 1.5–2 mm. Extrapolating the dependence $\Delta\lambda_{0.5} = f(I_p)$ (Fig. 4), we can assume that the lasing threshold for this system is reached at $I_p > (4-5)\times10^8$ W cm^{-2}. In this case, the value of l_g for the SiO_2 layers should decrease to ~350 μm; however, at such high pump radiation intensities, the destruction of the samples begins.

Note that the estimates $l_g \approx -\mu_a^{-1}$ obtained for the samples under study based on the maximum values of the spectral factor Ω_{max} at low intensities of pump radiation [$I_p < (1-5)\times10^5$ W cm^{-2}], corresponding to amplification of spontaneous emission are ~600–800 μm for SiO_2 layers and ~900–1200 μm for TiO_2 layers. An increase in I_p in the case of TiO_2 samples leads to a sharp increase in $\Omega(\lambda)$ in a narrow spectral band (565 nm $\leqslant \lambda \leqslant$ 577 nm), associated with the increasing contribution of induced fluorescence. One should also take into account the effect of a significant decrease in τ_{lt} with an increase in the pump intensity in such systems [21], which is described by changes in the Purcell factor [23] with increasing I_p. This factor, which characterises the kinetics of fluorescence decay for an elementary source located in a local volume playing the role of an optical resonator, is determined by the expression

$$F_P = \frac{3\lambda_c}{\Delta\lambda_c}\frac{(\lambda_c/n)^3}{4\pi^2 V}, \qquad (3)$$

where λ_c is the resonance wavelength; $\Delta\lambda_c$ is the width of the radiation spectrum; and V is the effective volume of the emitted mode [23]. Without going into details of determining the volume V, we note that, in accordance with [21], the presence of fluorophore molecules (rhodamine 6G) in a spatially limited highly scattering system (waveguide with an irregular structure) leads to a significant increase in the Purcell factor and, consequently, a decrease in the average lifetime of excited states by 2–6 times as compared to a free fluorophore. In our case, with an increase in I_p above the threshold lasing intensity in the TiO_2 layers, the $\lambda_c/\Delta\lambda_c$ ratio increases by 7–9 times (Fig. 4). Taking into account the increase in Ω_{max} in comparison with the subthreshold value, it can be assumed that at high pump radiation intensities, l_g significantly decreases.

Note that a similar effect in a much less pronounced form is also observed for SiO_2 layers at pump radiation intensities above $(3-4)\times10^6$ W cm^{-2}, (at $\tilde{I}_p > 6-7$, Fig. 7). Figure 10 shows model probability density functions of normalised propagation length of partial components of fluorescence $\rho(s/L)$ for SiO_2 and TiO_2 layers in the absence of amplification ($\mu_a = 0$, $l_g = \infty$). Obviously, for TiO_2 layers, the contribution of partial components with lengths $s \gg L$ in the fluorescence response will essentially increase even at a minor decrease in l_g. This behaviour can be interpreted as a manifestation of the quasi-waveguide effect [24] in the pumped fluorescent layers (less pronounced in the case of SiO_2 layers).

Before leaving the layer, the diffuse components of the fluorescence propagate along it over significant distances due to multiple repeated diffuse reflections from the boundaries into the bulk of the layer, and the negative absorption in the layer. However, an increase in r_f will at the same time lead to a reduction of the mean density of fluorescence energy in the layer, thus decreasing the slope of the $\tilde{r}_f = f(\tilde{I}_p)$ dependence. A mutual effect of these factors causes the empirical dependence $\tilde{r}_f \propto \tilde{I}_p^{\alpha}$ close to power one for the layers of TiO_2 (Fig. 7) with relatively small power exponent ($\alpha \approx 0.3$).

Note that the discrepancies between the model dependences $\tilde{r}_f = f(\tilde{I}_p)$ and the dependences obtained from experimental data (Fig. 7) are in good agreement with the experimentally observed features of the behaviour of the spectral characteristics of the fluorescence response ($\Delta\lambda_{0.5}$, Fig. 4 and Ω_{max}, Fig. 9) with increasing I_p. For TiO_2 layers, the model and experimental values of $\tilde{r}_f$ are comparable only in a narrow range of $\tilde{I}_p$ values near 1. As the pump intensity increases, the discrepancy between them rapidly increases, which correlates with a decrease in $\Delta\lambda_{0.5}$ and an increase in Ω_{max} and indicates a decrease in l_g. In the case of SiO_2 layers, a significant discrepancy between the model and experimental values of $\tilde{r}_f$ begins at $\tilde{I}_p \geqslant 6-7$. In this case, an increase in the rate of decrease in $\Delta\lambda_{0.5}$ and a slight increase in Ω_{max} also take place. Thus, the decrease in l_g with increasing pump intensity in this case is not as significant as for TiO_2 layers.

5. Conclusions

We found that in the regime of transition from spontaneous fluorescence to random lasing in pumped fluorescent randomly inhomogeneous layers, a quasi-waveguide effect is manifested due to the propagation of part of the fluorescent field diffuse components along the layers over considerable distances, essentially exceeding both the layer thickness and the pumped region size. A necessary condition for the manifestation of this effect is comparable values of the characteristic propagation length of radiation in the layer in the absence of amplification and the characteristic amplification length determined by the concentration of fluorophore molecules in the layer and the effective fluorescence cross section.

The effective fluorescence cross section depends on its spectral characteristics and the lifetime of excited fluorescent states, as well as on the optical transport parameters (in particular, on the transport length) of a randomly inhomogeneous matrix containing the fluorophore. It should be noted that even for 'soft' pump regimes (e.g., dc pumping of layers with small ratios of layer thickness to transport length), the criterion for the comparability of the characteristic propagation and amplification lengths can be achieved by increasing concentration of fluorophore molecules. This conclusion is confirmed by a comparison of the data presented in this work with the previously published results of reference-free low-coherence probing of TiO_2 and SiO_2 layers at higher concentrations (approximately 2.5×10^{-4} mol L^{-1} and higher) of rhodamine 6G [12, 13]. An increase in the contribution of stimulated radiation to the fluorescence response near and above the random lasing threshold, which occurs in the case of the TiO_2 layers under study, leads to a noticeable manifestation of the quasi-waveguide effect during radiation transfer in the layers.

The results obtained can be used to develop new approaches for laser diagnostics of randomly inhomogeneous media and composite materials.

Acknowledgements. This work was supported by the Russian Foundation for Basic Research (Grant No. 19-32-90221) in part of experimental research and statistical modelling and by the RF President's Grants Council (Grant No MK-2181.2020.2) in terms of design and manufacture of the experimental setup.

References

1. Pine D.J., Weitz D.A., Chaikin P.M., Herbolzheimer E. *Phys. Rev. Lett*., **60**, 1134 (1988).
2. Kim Y.L., Liu Y., Turzhitsky V.M., Roy H.K., Wali R.K., Backman V. *Opt. Lett*., **29**, 1906 (2004).
3. Yodh A., Chance B. *Phys. Today*, **48**, 34 (1995).
4. Lyubimov V.V. *Opt. Spectrosc*., **80**, 616 (1996) [*Opt. Spektrosk*., **80**, 687 (1996)].
5. Durduran T., Choe R., Baker W.B., Yodh A.G. *Rep. Prog. Phys*., **73**, 076701 (2010).
6. John S. *Phys. Rev. Lett*., **53**, 2169 (1984).
7. John S. *Phys. Today*, **44**, 32 (1991).
8. Wiersma D., Bartolini P., Lagendijk A., Righini R. *Nature*, **390**, 671 (1997).
9. Letokhov V.S. *Sov. Phys. JETP*, **26**, 835 (1968) [*Zh. Eksp. Teor. Fiz*., **53**, 1442 (1967)].
10. Noginov M.A. *Solid-State Random Lasers* (New York: Springer, 2005).
11. Ghulinyan M., Pavesi L. (Eds) *Light Localisation and Lasing: Random and Quasi-Random Photonic Structures* (Cambridge: Cambridge University Press, 2015).
12. Zimnyakov D.A., Yuvchenko S.A., Pavlova M.V., Alonova M.V. *Opt. Express*, **25**, 13953 (2017).
13. Zimnyakov D.A., Isaeva A.A., Isaeva E.A., Volchkov S.S. *Appl. Sci*., **10**, 1629 (2020).
14. Ishimaru A. *Wave Propagation and Scattering in Random Media* (New York: Academic, 1978; Moscow: Mir, 1981) Vol. 1.
15. Busch K., Soukoulis C.M., Economou E.M. *Phys. Rev. B*, **50**, 93 (1994).
16. Zimnyakov D.A., Pravdin A.B., Kuznetsova L.V., Kochubey V.I., Tuchin V.V., Wang R.K.,Ushakova O.V. *J. Opt. Soc. Am.*, **24**, 711 (2007).
17. Aull B.F., Jenssen H.P. *IEEE J. Quantum Electron*., **QE-18**, 925 (1982).
18. Zhu G., Small C.E., Noginov M.A. *J. Opt. Soc. Am. B*, **24**, 2129 (2007).
19. Noginov M.A., Zhu G., Bahoura M., Small C.E., Davison C., Adegoke J., Drachev V.P., Nyga P., Shalaev V.M. *Phys. Rev. B*, **74**, 184203 (2006).
20. Leupacher W., Penzkofer R. *Appl. Opt.*, **23**, 1554 (1984).
21. Gökbulut B., Naci I.M. *Opt. Express*, **27**, 15996 (2019).
22. Wiersma D.S., Lagendijk A. *Phys. Rev. E*, **54**, 4256 (1996).
23. Purcell E.M. *Phys. Rev*., **69**, 1 (1946).
24. Zimnyakov D.A., Sina D.S., Yuvchenko S.A. et al. *Quantum Electron*., **44,** 59 (2014) [*Kvantovaya Elektron*., **44**, 59 (2014)].